A contactless inductive velocity reconstruction method for metallic and semiconducting melts

Frank Stefani and Gunter Gerbeth
Forschungszentrum Rossendorf, MHD Department,
PO Box 510119, Dresden D-01314, Germany

Abstract

The knowledge of the flow in metallic and semiconducting melts is important for a number of industrial problems. Optical methods cannot be applied due to the opaqueness of those fluids. Ultrasonic methods have problems with wetting and thermal stability when applied in hot metallic melts. Evidently, contactless methods for velocity determination would be highly desirable. In some applications even a coarse knowledge of the flow topology and the direction of the main eddies would be of high value. We study the possibility of velocity reconstruction in electrically conducting fluids from external measurements of different induced magnetic fields. It is shown that for a reliable velocity reconstruction the effect of the electric potential at the fluid boundary on the induced magnetic field should be taken into account.

Keywords: Inverse problems; crystal growth, metallurgy

1 Introduction

In a number of technologies including metal casting and crystal growth it is often important to have some knowledge of the velocity fields in liquid metals or semiconductor melts. Unfortunately, the opaqueness of those fluids forbids the use of optical measurement techniques, e.g. the Laser-Doppler Anemometry [1] or the Particle Image Velocimetry [2]. The application of ultrasound techniques [3] or of special probes (pressure probes, potential probes, mechano-optical probes etc.) is also not trivial, because the considered melts are often very hot and/or chemically aggressive. A method that would allow the contactless determination of the velocity would be very desirable, even if it could provide only a rough picture of the velocity structure.

The electromagnetic induction principle has been used for a long time to determine the mean volume flow in pipes from electric potential measurements at some boundary points (see, e.g., the classical monographs [4, 5]). Recent error reducing refinements of this method include the successive use of different external magnetic fields [6, 7].

The axial velocity component in pipe flows is, however, not the only interesting quantity. In a number of technological processes one is interested in the full three-dimensional distribution of the velocity vector field. One example is the Czochralski crystal growth technique. For growing large diameter crystals magnetic fields are frequently used to control the distributions of oxygen and dopants by influencing the motion of the silicon melt [8, 9]. In this context, different magnetic field configurations are being discussed, e.g. axial and cusp fields which can be produced by the same Helmholtz coil pair using equal and opposite current directions in the coils, respectively. Applied magnetic fields are already an intrinsic element of the process, hence it is quite natural to ask for measurement techniques in which these fields are utilized. If it were possible for given applied magnetic fields to reconstruct the three-dimensional velocity distribution from induced magnetic fields, a re-active control of the melt flow by changing the external fields could also be conceivable.

What are, from a topological point of view, the main differences and similarities between pipe flow and three-dimensional velocity reconstruction? In pipe flows one tries to reconstruct at most the cross-sectional, i.e., a two-dimensional distribution of one (the axial) velocity component. Suppose that one homogeneous magnetic field is applied and that the Fourier coefficients of the circumferential electric potential are determined. Then it is only possible to compute certain radial moments of the Fourier coefficients of the axial velocity field [10]. For a flow in a closed vessel we can assume that the three-dimensional velocity field has been parameterized by two scalar functions (making use of the incompressibility of the fluid). Obviously, for the determination of these two functions one should also have two sets of information measured outside, and in correspondence with the pipe flow case one should expect also a radial ambiguity of the solution.

Three-dimensional inductive velocity reconstruction was the topic of three recent papers [11, 12, 13]. In [11, 12] we have addressed the problem of spatial velocity reconstruction in conducting fluids from magnetic field and electric potential measurements. The currents proportional to the cross-product of velocity and magnetic field give rise to an additional magnetic field measurable outside the fluid volume and to an electric potential measurable at the fluid boundary.

In [13] we have considered the case of using two sets of measured induced magnetic fields instead of one set of magnetic fields together with one set of electric potentials. This contactless method is especially interesting for those applications in which the electric potential measurement at the fluid boundary is hard to manage. This is particularly important for hot and aggressive fluids or for facilities where the fluid boundary is not accessible for technological reasons.

In this paper we will present a numerical implementation of the basic idea formulated in [13]. In the second section, the underlying theory is delineated. A numerical example of the forward and the inverse problem is presented in the third section. In the fourth section, we sketch an experiment which is currently under construction in order to put the theory of the method into laboratory practice. The paper finishes with some concluding remarks.

2 Basics

Suppose a fluid of electrical conductivity σ, moving with the stationary velocity $\mathbf{v}$, is exposed to an externally applied steady magnetic field $\mathbf{B}_0$. Then a current density $\mathbf{j}$ is induced which is governed by Ohm's law

$$\mathbf{j} = \sigma(-\nabla\varphi + \mathbf{v} \times \mathbf{B}) \tag{1}$$

with φ denoting the electric potential. In general, the magnetic field $\mathbf{B}$ in Eq. 1 has to be understood as the sum $\mathbf{B} = \mathbf{B}_0 + \mathbf{b}$, where $\mathbf{b}$ is the induced magnetic field. The amplitude of the induced magnetic field is of the order $O(R_m B_0)$ where the magnetic Reynolds number is defined by $R_m = \mu_0 \sigma l v$ (l is a typical length scale, v a typical velocity of the flow). This induced magnetic field can be calculated by means of Biot-Savart's law

$$\begin{aligned} \mathbf{b}(\mathbf{r}) &= \frac{\mu_0\sigma}{4\pi}\int\limits_V \frac{(\mathbf{v}(\mathbf{r}') \times \mathbf{B}(\mathbf{r}')) \times (\mathbf{r}-\mathbf{r}')}{|\mathbf{r}-\mathbf{r}'|^3} dV' \\ &\quad -\frac{\mu_0\sigma}{4\pi}\int\limits_S \frac{\varphi(\mathbf{s}')\mathbf{n}(\mathbf{s}') \times (\mathbf{r}-\mathbf{s}')}{|\mathbf{r}-\mathbf{s}'|^3} dS' \,. \end{aligned} \tag{2}$$

The first term on the r.h.s of Eq. 2 represents the effect of the *impressed* or *primary* currents $\sigma\mathbf{v} \times \mathbf{B}$ in the fluid volume V. The second term arises if we convert the volume integral over the $\nabla\varphi$ term into a boundary integral. These so-called *secondary* currents depend on the electrostatic potential at the fluid boundary S. The electric potential φ, in turn, has to fulfill the boundary integral equation

$$\begin{aligned} \varphi(\mathbf{s}) &= -\frac{1}{2\pi}\int\limits_V \frac{(\mathbf{v}(\mathbf{r}') \times \mathbf{B}(\mathbf{r}')) \cdot (\mathbf{s}-\mathbf{r}')}{|\mathbf{s}-\mathbf{r}'|^3} dV' \\ &\quad +\frac{1}{2\pi}\int\limits_S \frac{\varphi(\mathbf{s}')\mathbf{n}(\mathbf{s}') \cdot (\mathbf{s}-\mathbf{s}')}{|\mathbf{s}-\mathbf{s}'|^3} dS' \,, \end{aligned} \tag{3}$$

which results from Green's theorem for the solution of the Poisson equation for the case of insulating boundaries.

These two Eqs. 1 and 2 for $\mathbf{b}(\mathbf{r})$ and $\varphi(\mathbf{s})$ are valid for arbitrary values of the magnetic Reynolds number R_m (at least if no oscillatory solutions appear which would require a modification of the formulae). For large R_m, they constitute the integral equation formulation for steady dynamos in finite domains [14]. For the industrially interesting case of small R_m, however, the induced magnetic fields in the volume integrals on the right-hand sides can be neglected and the total $\mathbf{B}$ can be replaced by $\mathbf{B}_0$.

The main result of the papers [11] and [12] was that the velocity structure of the flow can be reconstructed from the external measurement of an appropriate component of the induced magnetic field (e.g., the radial component for a spherically shaped fluid volume) and the electric potential at the fluid boundary, apart from an uncertainty in the radial distribution of the flow.

The theoretical advantage of this method is that the electric potential in Eqs. 2 and 3 at the boundary is known from measurement. The disadvantage of this method is that one needs a contact with the fluid. The following considerations are concerned with the question how the missing electric potential information can be compensated by additional magnetic field information, and how the apparent necessity to know φ at the boundary can be circumvented.

The main idea is to use two external magnetic fields, differing in their direction, and to measure the two corresponding sets of induced magnetic fields [13]. However, the main obstacle for the application of this method is the unknown electric potential at the boundary, which cannot be longer considered as known by measurement. There is one exceptional case in which this problem does not appear. Suppose that the fluid volume is spherical and that we measure the radial component of the induced magnetic field. Multiplying Eq. (2) with the unit vector in radial direction, $\mathbf{r}/r$, we see that the second term on the r.h.s vanishes due to the identities $(\mathbf{n}(\mathbf{s}') \times \mathbf{r}) \cdot \mathbf{r} = 0$ and $\mathbf{n}(\mathbf{s}') \times \mathbf{s}'$, the latter identity being only valid in the spherical case. For any other than spherical fluid volumes, there will always be an influence of the boundary currents on any chosen magnetic field component. One can try to keep this influence small, e.g. by choosing the magnetic field component orthogonal to the next surface element. Nevertheless, for other than spherical geometry it will be wise to take the influence of secondary currents into account. But how to do that, without knowing the electric potential?

For the solution of this puzzle, let us assume certain spatial discretizations of the magnetic field data, of the desired velocity in the volume, and of the electric potential at the boundary. The measured data are collected into a vector with a total of NB entries $b_i^{(B_1,B_2)}$, $i = 1...NB$ where (B_1, B_2) denotes the measured values for the first and the second applied magnetic field. The electric potential is discretized at NP points at the fluid boundary, $\varphi_k^{(B_1,B_2)}$, $k = 1...NP$ and (B_1, B_2) denoting again the values for the first and the second applied magnetic field. The velocity is collected into a vector with NV entries v_n, $n = 1...NV$.

Then, Eqs. (2) and (3) can be rewritten in the following way:

$$
\begin{aligned}
b_i^{(B_1,B_2)} &= R_{in}^{(B_1,B_2)} v_n + S_{ik} \varphi_k^{(B_1,B_2)} \ , && (4) \\
\varphi_k^{(B_1,B_2)} &= T_{kn}^{(B_1,B_2)} v_n + U_{kk'} \varphi_{k'}^{(B_1,B_2)} \ . && (5)
\end{aligned}
$$

The matrix elements $R_{in}^{(B_1,B_2)}$, S_{ik}, $T_{kn}^{(B_1,B_2)}$, and $U_{kk'}$ can be directly inferred from Eqs. (2) and (3). Note that only $R_{in}^{(B_1,B_2)}$ and $U_{in}^{(B_1,B_2)}$ depend on the direction of the applied magnetic field whereas S_{ik} and $U_{kk'}$ depend only on the geometry of the fluid volume.

The crucial point is now that Eq. (5) can be solved for the electric potential, although in a non-trivial manner. The difficulty comes from the problem that the matrix $I - U$ (I is the unity matrix) is singular; a consequence of the fact that a shift of the electric potential is physically irrelevant. In order to get a sensible inversion of the Matrix $I-U$ one can use the deflation technique which was developed in [15] (see also [16]). If we denote the inverse of the deflated Matrix $I-U$ by $(I-U)^{-1,defl}$ we can get the following linear connection between the velocity and the magnetic field

$$b_i^{(B_1,B_2)} = R_{in}^{(B_1,B_2)} v_n + S_{ik'}((I-U)^{-1,defl})_{k'k} T_{kn}^{(B_1,B_2)} v_n \; . \qquad (6)$$

Evidently, Eq. 6 comprises two parts of the influence of the velocity on the magnetic field. The first one reflects the direct induction of the primary currents, the second one gives the induction effect mediated by the secondary currents. The calculation of the matrix elements $S_{ik'}((I-U)^{-1,defl})_{k'k} T_{kn}^{(B_1,B_2)}$ needs some numerical effort since it is recommendable to use a fine discretization of the fluid boundary, i.e. a high number of NP, for the solution of the boundary integral equation 3. However, for the practical implementation it is of high importance that this matrix must be calculated only once for every applied magnetic field. As a result we get a rather modest number of matrix elements that reflect the boundary mediated induction of a few (typically NV will be in the order of 10...100) velocity degrees of freedom on a few (typically NB will also be of the order 10..100) measured magnetic field data.

3 A numerical example

In the following, the forward and the inverse problem will be illustrated for a simple velocity example which has some relevance for the experiment that will be discussed in the next section. In a cylinder of height and diameter equal to 1 we consider a velocity field $\mathbf{v}$ whose components are given by $v_r = -r(2r-1)\cos(\pi z)$, $v_\phi = 5 \cdot r(0.5-r)\sin(\pi z)$, $v_z = (6r-2)\sin(\pi z)/\pi$. This velocity field contains a poloidal and a toroidal part. Some streamlines of the velocity field field are depicted in Fig. 1a.

For the primary magnetic fields we assume $\mathbf{B}_{01} = B_0 \mathbf{e}_x$ and $\mathbf{B}_{02} = B_0 \mathbf{e}_z$. The computed magnetic fields that are induced at a total of 78 points covering the surface of the cylinder are shown in the remaining parts of Fig. 1. For the forward computation, the fluid volume has been discretized by 20x24x24 points in radial, azimuthal, and axial direction, respectively. Figs. 1b and 1c show the induced magnetic fields for $\mathbf{B}_{01} = B_0 \mathbf{e}_x$, with the difference that Fig. 1b shows the induction effect from the primary currents only (i.e., the first term on the r.h.s of Eqs. 2 and 6), whereas Fig. 1c shows the full induced field when the secondary currents (the second term on the r.h.s of Eq. 2 and 6) are taken into account correctly. The effect of the secondary currents is nicely visible in Fig. 1d and Fig. 1e, which show the induced fields for $\mathbf{B}_{02} = B_0 \mathbf{e}_z$. The magnetic field in Fig. 1d comprises a rotational component that is, however, unphysical because the magnetic field in the exterior must be curl-free due to $\nabla \times \mathbf{B} = \mu_0 \mathbf{j} = 0$. This unphysical rotational component disappears in Fig 1e where the effect of the secondary currents has been taken into account correctly.

In the following we evaluate the error that appears in the determination of the magnetic field if we skip the effect of the secondary currents. We consider a more or less realistic measurement configuration. The arrows in Figs. 2a and 2b indicate the directions of the magnetic field components which we assume to be measured. The choice of these components was dictated by the guess that the normal component close to the boundary should be less affected by the boundary term than the tangential components (remind our argument from section 2 that for spherical domains the radial component is completely unaffected). It turns out that for the $\mathbf{B}_{02} = B_0 \mathbf{e}_z$ this choice of the magnetic field components makes the effect of the secondary currents irrelevant, as they influence in this case only the rotational component and not the radial and axial component.

However, for $\mathbf{B}_{01} = B_0 \mathbf{e}_x$ the situation is quite different. The grey scale in Fig. 2a shows the actual value of the induced magnetic field components to be measured, the grey scale in Fig. 2b shows the deviation (in percent) from the correct values which appears if we skip the secondary currents. As expected from geometric arguments, the deviations are highest close to the edges of the cylinder whereas they are more moderate close to the centers of the top and the bottom and the cylindrical surface.

Having established a linear connection between the desired velocity field and the measured magnetic fields (Eq. 6) that takes into account the secondary currents without measuring the electric potential, we start to infer the velocity field by means of standard inversion methods.

The problem that still remains is the non-uniqueness of the inverse problem, i.e., the fact that there is a wide variety of velocity configurations which cannot be distinguished by their induced magnetic fields. For a spherical fluid domain we had shown [12, 13] that this non-uniqueness concerns the radial dependence of the velocity field. It is reasonable to believe that this result can be generalized to similar compact fluid domains, such as cylinders with aspect ratios close to one. There is a chance to resolve this non-uniqueness with regard to the depth of the fluid by using time dependent primary fields, but this is not the subject of the present paper. Here we simply use the regularization method in order to select from many possible solutions those with a high physical plausibility.

In practice we apply the so-called Tichonov regularization and the method of Tichonov's L-curve [17]. Note that the inversion of Eq. 6 is equivalent to the minimization of the mean quadratic deviation of the measured fields from the fields resulting from the supposed velocity distribution. Regularization means that we add to the functional of mean quadratic deviation one or more *penalty functions* which are chosen, for convenience, as quadratic functionals of the velocity. For our purpose we minimize the functional

$$F[\mathbf{v}] = F_{B_x}[\mathbf{v}] + F_{B_z}[\mathbf{v}] + F_{div}[\mathbf{v}] + F_{pen}[\mathbf{v}] \tag{7}$$

with

$$F_{B_x}[\mathbf{v}] = \sum_{i=1}^{NB} \frac{1}{\sigma_{i,B_x}^2} \left(b_{i,meas}^{(B_x)} - b_{i,comp}^{(B_x)}[\mathbf{v}] \right)^2 \tag{8}$$

$$F_{B_z}[\mathbf{v}] = \sum_{i=1}^{NB} \frac{1}{\sigma_{i,B_z}^2} \left(b_{i,meas}^{(B_z)} - b_{i,comp}^{(B_z)}[\mathbf{v}] \right)^2 \tag{9}$$

$$
\begin{aligned}
F_{div}[\mathbf{v}] &= \frac{1}{\sigma_{div}^2} \sum_{k=1}^{NV} (\nabla \cdot \mathbf{v})_k^2 \, \Delta V_k &\quad (10) \\
F_{pen}[\mathbf{v}] &= \frac{1}{\sigma_{pen}^2} \sum_{k=1}^{NV} \mathbf{v}_k^2 \Delta V_k &\quad (11)
\end{aligned}
$$

Evidently, $F_{B_x}[\mathbf{v}]$ and $F_{B_x}[\mathbf{v}]$ are the mean squared residual deviation of the measured magnetic fields. $F_{div}[\mathbf{v}]$ enforces the divergence of the velocity field to be (more or less) zero, and $F_{pen}[\mathbf{v}]$ is the penalty functional which tries to keep the mean quadratic velocity more or less small. The parameters σ_{i,B_x} and σ_{i,B_z} are a-priori errors assumed for the individual measurements of the components $b_{i,meas}^{(B_x)}$ and $b_{i,meas}^{(B_z)}$ for the two different applied magnetic fields. In our numerical example they are set to one. The parameter σ_{div} is a measure for how much divergence we allow for the velocity field; we chose it very small. The main parameter to play with is σ_{pen} the inverse of which is usually called the regularization parameter. If we scale σ_{pen} from very low to very high values the minimization of the total functional (9) will give solutions with increasing quadratic norm.

In our example, the inverse problem is solved with a discretization of the fluid volume by 5x6x4 points in radial, azimuthal, and axial direction respectively. Note that this discretization is much coarser than the discretization for the forward problem. We consider the magnetic field data as they came out of the forward problem as “measured” data, and try to infer from these “measured” data the velocity field. Figure 3 shows the dependence of several quantities on the choice of σ_{pen} . As the abscissa we chose the mean quadratic norm of the velocity field which increases with increasing σ_{pen} (cf. Eq. 11). Fig. 3a shows the rms deviation of the “measured” magnetic fields from the magnetic fields arising from the velocity solution, Fig. 3b shows the empirical correlation coefficient of the resulting velocity field the with analytically given velocity field which was supposed in the forward problem, and Fig. 3c gives the mean value of the velocity field (not weighted by the volume). In every plot, there are two curves that correspond to the solution with and without consideration of the secondary currents. Although not very pronounced, we see the ”knee” in the Tichonov curve that indicates a physically sensible result. At this point the correlation coefficient for the inversion with considering the boundary term reaches a maximum of 0.86 which is a good result for this kind of inverse problem. To judge this result one should note again that the discretization for the inverse problem is much coarser than the discretization for the forward problem. In contrast to that good result the inversion without considering the secondary currents has a pathological behaviour, with a correlation coefficient that becomes even negative.

In summary, we conclude that for the contactless inductive velocity reconstruction in non-spherical volumes it is of great value to take into account the electric potential effect from the boundary. This method can be numerically implemented in a cheap way by solving the (geometry dependent) boundary integral equation only once which leaves a matrix of moderate order to be inverted. It provides reliable estimates of the velocity field. A simpler method, which tries to avoid the solution of the boundary integral equation, yields much worse results, even if the direction of the measured magnetic field components is chosen wisely.

4 An experimental setup

From the analytical and numerical point of view, the contactless inductive velocity reconstruction method promises reasonable results. However, before thinking of industrial applications, an experiment should be carried out in order to check possible pitfalls of the method. Difficulties may arise from instationary flows, from magnetic stray fields, and from the limited sensitivity of the magnetic field sensors. In this context one should always keep in mind that the induced magnetic fields are much smaller than the applied magnetic fields.

In Fig. 4 we show the design principle of our experiment. A conducting fluid in a cylinder is stirred by a motor driven propeller that produces a mix of poloidal and toroidal motion. Two Helmholtz coil pairs are switched on and off producing two different external magnetic fields pointing alternatingly in x and z direction. Note that it is also possible to work with one single Helmholtz coil pair which can produce a rather homogeneous field in one direction or a so-called cusp-field, when the current directions in the two coils are the same or opposite, respectively.

Such an experiment is presently under construction. We use InGaSn as conducting fluid which is liquid at room temperature and has a reasonable electrical conductivity ($\sigma = 3.3 \cdot 10^6 (\Omega m)^{-1}$). The cylinder has a diameter of 0.2 m and the height of the liquid is also 0.2 m.

Fig. 5 shows the cylindrical vessel with the fluid, the motor, and some circuit boards bearing 8 Hall sensors each together with the AD-transformer. A total of 48 Halls sensors is planned to cover the cylinder.

First pre-experiments have shown that the induced magnetic fields can indeed be detected on the back-ground of much stronger applied fields.

5 Conclusions and prospects

In this paper, we have delineated the basics of a contactless inductive velocity reconstruction method for flows in liquid metals and semiconducting melts. We have shown that numerically the method provides reasonable results, and we have sketched a liquid metal experiment were this method will be tested. A lot of work remains to be done in order to adapt the method to real-world applications in industry.

References

[1] Tropea, C. Laser-Doppler anemometry - recent developments and future challenges. Meas. Sci. Tech. **1995**, *6*, 609–619.

[2] Stanislas, M.; Kompenhans, J.; Westerweel, J. (Eds.) *Particle Image Velocimetry - Progress Towards Industrial Application*; Kluwer, Dordrecht, 2000.

[3] Hauptmann, P.; Hoppe, N.; Püttner, A. Application of ultrasonic sensors in the process industry. Meas. Sci. Tech. **2002**, *13*, R73–R83.

[4] Shercliff, J. A. *The Theory of Electromagnetic Flow-Measurement*; Cambridge University, Cambridge, 1987.

[5] Schommartz, G. *Induktive Strömungsmessung*; Technik, Berlin, 1974.

[6] Horner, B.; Mesch, F.; Trächtler, A. A multi-sensor induction flowmeter reducing errors due to non-axisymmetric flow profiles. Meas. Sci. Tech. **1996**, *7*, 354–360.

[7] Tu Y. X.; Wernsdoerfer, A.; Honda, S.; Tomita, Y. Estimation of Conduction Velocity Distribution by Regularized–Least–Squares Method. IEEE Trans. Biomedical Engineering **1997**, *44*, 1102-1106.

[8] Hurle, D. T. J.; Series, R. W. Use of magnetic fields in melt growth. In *Handbook of Crystal Growth,* Hurle, D. T. J., Ed., North-Holland, 1994, Pt. 2a, 259-285.

[9] Galindo, V.; Gerbeth, G.; von Ammon, W.; Tomzig, E.; Virbulis, J. Crystal growth melt flow control by means of magnetic fields. Energ. Convers. Manage. **2002**, *43*, 309–316.

[10] Engl, W. Der induktive Durchflußmesser mit inhomogenem Magnetfeld. Arch. Elektrotechnik. **1970**, *53*, 344–359.

[11] Stefani, F; Gerbeth, G. Velocity reconstruction in conducting fluids from magnetic field and electric potential measurements. Inverse Problems **1999**, *15*, 771–786.

[12] Stefani, F; Gerbeth, G. On the uniqueness of velocity reconstruction in conducting fluids from measurements of induced electromagnetic fields. Inverse Problems **2000**, *16*, 1–9.

[13] Stefani, F; Gerbeth, G. A contactless method for velocity reconstruction in electrically conducting fluids. Meas. Sci. Tech. **2000**, *11*, 758–765.

[14] Stefani, F; Gerbeth, G.; Rädler, K.-H. Steady dynamos in finite domains: an integral equation approach. Astron. Nachr. **2000**, *321*, 65–73.

[15] Barnard, A. C. L.; Duck, I. M.; Lynn, M. S.; Timlake, W. P. The application of electromagnetic theory to electrocardiology. II. Numerical solution of the integral equation. Biophys. J. **1967**, *7*, 463-491.

[16] Hämäläinen, M.; Hari, R.; Ilmoniemi, R. J.; Knuutila, J.; Lounasmaa, O. V. Magnetoencephalography - theory, instrumentation, and application to noninvasive studies of the working human brain. Rev. Mod. Phys. **1993**, *65*, 413–497.

[17] Hansen, P. C. Analysis of discrete ill-posed problems by means of the L-curve. SIAM Review **1992**, *34*, 561-580.

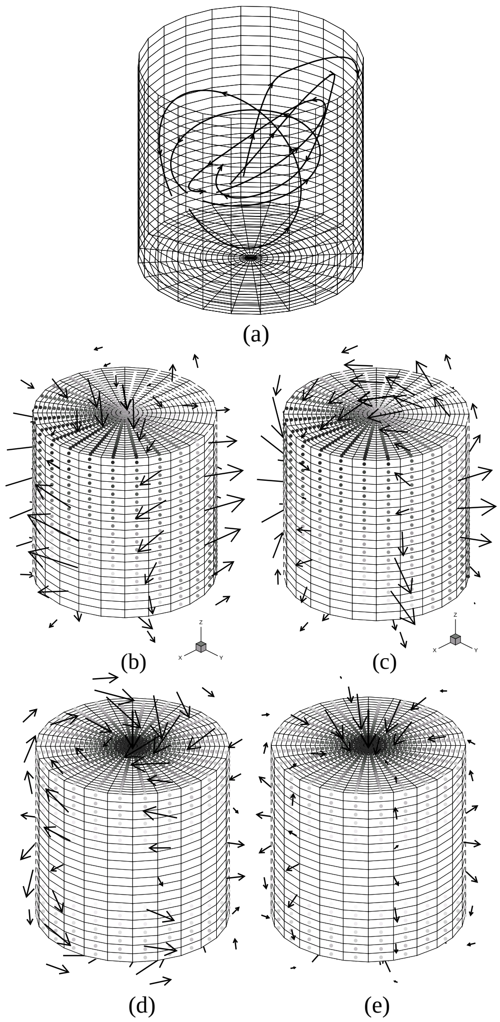

Figure 1: The forward problem. (a) The assumed velocity field, comprising a toroidal and a poloidal component. (b) Induced magnetic field for $\mathbf{B}_0 = B_0\mathbf{e}_x$, without considering the boundary potential. (c) Induced magnetic field for $\mathbf{B}_0 = B_0\mathbf{e}_x$, with considering the boundary potential. (d) and (e) are the same as (b) and (c), respectively, but for $\mathbf{B}_0 = B_0\mathbf{e}_z$. The grey scale of the small bullets in the surface elements denotes the computed electrical potential which is, however, not an observable for the inverse problem.

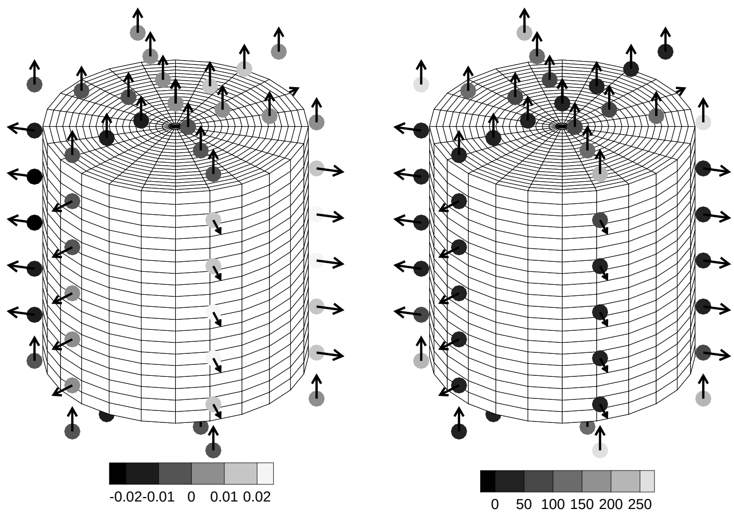

(a) (b)

Figure 2: Illustration of the error that appears when the secondary currents are skipped. (a) The induced magnetic field components for $\mathbf{B}_0 = B_0\mathbf{e}_x$, as they result from the solution of the forward problem. The arrows show the chosen field direction to be measured, the grey scale gives the value of the measured component. (b) Differences between the values with and without considering the boundary term. The arrows show the chosen field direction, the grey scale gives the relative deviation in per cent.

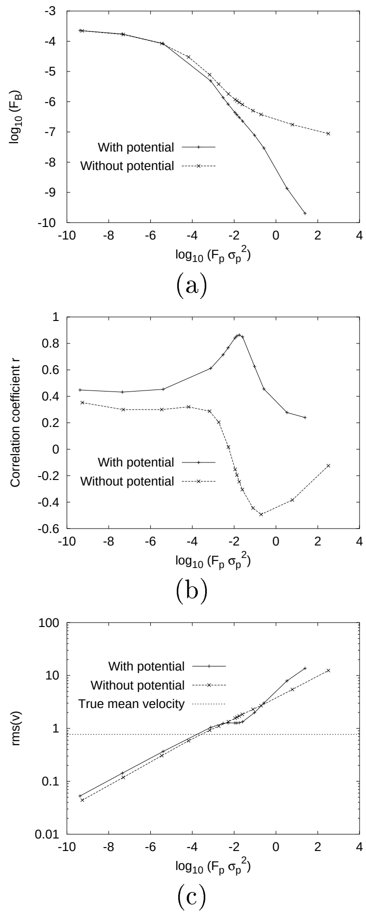

Figure 3: Solution of the inverse problem with and without considering the electric potential term at the boundary. (a) rms deviation of the measured magnetic fields from the modeled ones. (b) Empirical correlation coefficient of the true velocity and the modeled velocity. (c) rms of the modeled velocity, compared with the true value.

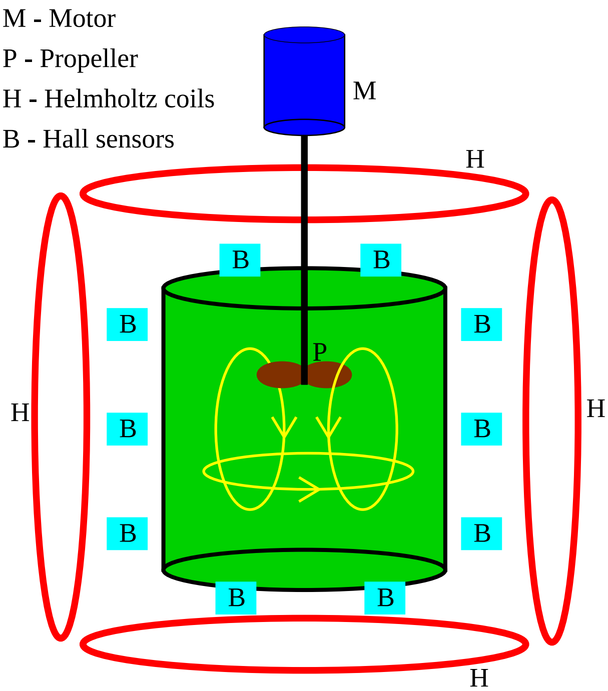

Figure 4: The principle of the experiment. In a cylindrical vessel of 0.2 m diameter a liquid metal (InGaSn) is stirred by a motor driven propeller. Two Helmholtz coils are used to produce external magnetic fields in x and z direction. The induced magnetic fields are measured by Hall sensors positioned outside the vessel.

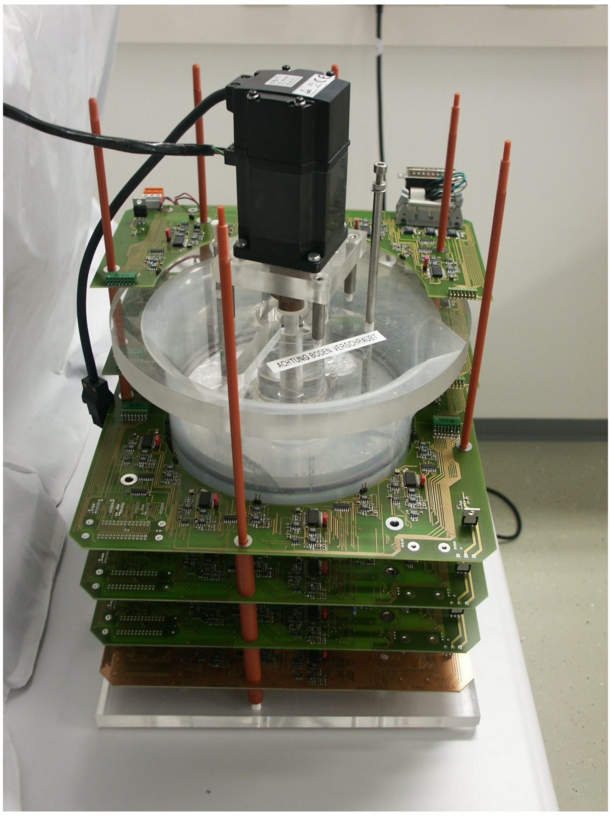

Figure 5: The experimental setup, with the Hall sensors and the AD transformers.